Review article

Xing Liu, Qun Gao, Yang Zheng, Dong Mao* and Jianlin Zhao

Recent progress of pulsed fiber lasers based on transition-metal dichalcogenides and black phosphorus saturable absorbers

https://doi.org/10.1515/nanoph-2019-0566
Received December 30, 2019; revised February 4, 2020; accepted February 4, 2020

Abstract: Transition-metal dichalcogenides (TMDCs) and black phosphorus (BP) are typical 2D materials with layer-dependent bandgaps, which are emerging as promising saturable absorption materials for pulsed fiber lasers. In this review, we discuss the nonlinear saturable absorption properties of TMDCs and BP, and summarize the recent progress of saturable absorbers from fabrication methods to incorporation strategies. The performances of saturable absorbers and the properties of Q-switched/mode-locked fiber lasers at different wavelengths are summarized and compared to give a comprehensive insight to optical modulators based on TMDCs/BP, and to promote their practical applications in nonlinear optics.

Keywords: transition-metal dichalcogenides; black phosphorus; saturable absorber; mode-locked fiber laser; Q-switched fiber laser.

1 Introduction

Attributed to their unique properties of compact structure, good flexibility, and low cost, pulsed fiber lasers are excellent light sources for various applications, such as optical communications [1, 2], biological photonics [3, 4], laser micromachining [5, 6], etc. Passive Q-switching and mode-locking techniques are two common methods for generating pulsed lasers, with the key component of a saturable absorber (SA). Several types of techniques or elements, including a semiconductor SA mirror (SESAM) [7, 8], nonlinear polarization rotation [9, 10], carbon nanotubes [11, 12], and a nonlinear optical loop mirror (NOLM) [13, 14] have been developed to shorten the pulse for generating Q-switched or mode-locked lasers.

In the past several decades, the most famous SA, SESAM, has been widely used in commercial laser systems. However, SESAMs also suffer from a narrow operating bandwidth, low damage threshold, and complex preparation process. Those limitations motivate researchers to search for new types of SAs for pulsed lasers. Recently, 2D materials revolutionized the study from nonlinear optics [15], optoelectronics [16–21], medical treatment [22–24], and energy storage [25–27] attributing to their remarkable physical properties and the unique dimensionality effect [28, 29]. These 2D materials usually exhibit layered structures in which weak Van der Waals forces stabilize the stacking of layers and strong covalent bonds join together atoms in-plane. As a result, they can be exfoliated into single-layer or few-layer nanosheets that have the advantages of a fast recovery time, ease of preparation and integration to a fiber system. The most well-known 2D material is graphene, which was demonstrated by Novoselov et al. [30] using the mechanical exfoliation (ME) approach. Single-layer graphene is composed of a single-atom layer of carbon forming a 2D honeycomb lattice. Bao et al. [31] and Hasan et al. [32] have demonstrated mode-locked erbium-doped fiber lasers (EDFLs) based on a few-layer graphene SA.

Motivated by the progress of a graphene SA, researchers have developed a host of graphene-like materials and explored their applications in pulsed fiber lasers from visible, near-infrared to mid-infrared wavelength [33–35]. A topological insulator [36–38] is a new state of quantum matter that has an insulating bulky gap, and a gapless edge state or surface state. Several types of topological

***Corresponding author: Dong Mao,** MOE Key Laboratory of Material Physics and Chemistry under Extraordinary Conditions, and Shaanxi Key Laboratory of Optical Information Technology, School of Physical Science and Technology, Northwestern Polytechnical University, Xi’an 710129, China, e-mail: maodong@nwpu.edu.cn. https://orcid.org/0000-0002-8466-0430
Xing Liu, Qun Gao, Yang Zheng and Jianlin Zhao: MOE Key Laboratory of Material Physics and Chemistry under Extraordinary Conditions, and Shaanxi Key Laboratory of Optical Information Technology, School of Physical Science and Technology, Northwestern Polytechnical University, Xi’an 710129, China

insulators such as Bi_2Te_3, Sb_2Te_3 and Bi_2Se_3 have been proved to exhibit a broadband saturable absorption property [39] and Q-switched or mode-locked fiber lasers have been reported at 1.06 µm [40, 41], 1.55 µm [42, 43], and 2 µm [44, 45].

After that, another type of 2D material, transition-metal dichalcogenides (TMDCs) [46–49], has attracted rising attention due to the layer-dependent bandgap and high nonlinear optical response. TMDCs are a family of anisotropic semiconductor materials with the common chemical formula of MX_2, in which X is a group VI element (i.e. S, Se, Te) and M is a transition metal (i.e. Mo, W). By using single-layer or few-layer TMDCs as a nonlinear medium, several typical nonlinear phenomena have been reported, such as second harmonic generation [50, 51], saturable absorption [52–54], and two-photon absorption [55, 56]. The bandgap and stability of TMDCs decrease as the mass of the chalcogen atom increases from S, Se to Te [57]. However, the bandgap of typical TMDCs is still higher than 0.7 eV, which is still far away for the mid-infrared waveband [58–60].

In recent years, some 2D monoelemental materials such as phosphorene [61], arsenene [62], antimonene [63], and bismuthene [64] have also attracted great interest owing to their extraordinary physical properties. Especially, black phosphorus (BP) [65–69], the most thermodynamically stable allotrope of the element phosphorus, has a layer-dependent bandgap from 0.3 eV (bulk) to 2.0 eV (monolayer) [70, 71], which covers the vacancy between zero-bandgap graphene and large-bandgap TMDCs (e.g. 1.29~1.8 eV for MoS_2) [72]. Thus, BP is a promising nonlinear optical material at the mid-infrared range that is beyond the absorption wavelength of TMDCs [66, 73–78]. In addition to these famous 2D materials, several new materials such as tin sulfide [79, 80] and perovskite [81–83], were also found to exhibit a saturable absorption property.

As aforementioned, graphene and topological insulators can be categorized as Dirac materials that have zero bandgaps [84–86]. The preparation of graphene and topological insulators, as well as their applications in pulsed lasers, have been discussed and summarized by several exhaustive reviews and articles [37, 39, 87–91]. Unlike zero-bandgap materials, TMDCs and BP benefit from the layer-dependent bandgap, and their nonlinear optical properties are more complex and interesting [15, 66, 92, 93]. Here, we review these important advances of pulsed fiber lasers based on TMDCs and BP SAs. The nonlinear optical properties and fabrication methods of two types of SA are discussed and compared to give a comprehensive insight to optical modulators based on 2D materials. The performances of Q-switched and mode-locked fiber lasers at different wavelengths are also summarized in this review.

2 Fabrication and characterization of TMDCs and BP SAs

2.1 Fabrication methods

As illustrated in Figure 1, there are two main methods for preparing 2D materials: the top-down method [94] and the bottom-up method [95]. The top-down method includes ME and liquid-phase exfoliation (LPE) [96, 97] by destroying the van der Waals forces to fabricate single-layer or few-layer 2D materials. The bottom-up method grows nanomaterials on a molecular level utilizing chemical or physical reactions, such as chemical vapor deposition (CVD) [98, 99], molecular beam epitaxy [100, 101], hydrothermal synthesis [102, 103], pulse magnetron sputtering [104, 105], pulsed laser deposition [106, 107], etc. Here, we give a simple introduction to ME, LPE and CVD, which are three widely used methods for preparing 2D materials including TMDCs and BP.

The ME method has been widely used to fabricate 2D nanomaterials since the first successful exfoliation of graphene in 2004 by Novoselov et al. [30]. After that, few-layer or single-layer topological insulators, TMDCs, and BP were obtained by using a similar approach. In the ME process, adhesive tape is used to exfoliate bulk layered crystals down to monolayer and few-layer nanosheets. The ME method can produce high-quality 2D nanomaterials for fundamental research, but the efficiency is extremely low, which limits its realistic applications.

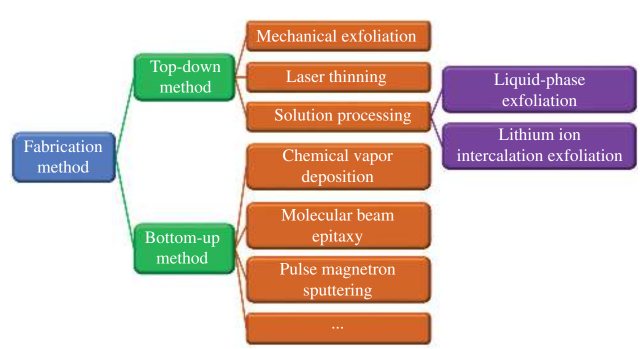

Figure 1: Typical fabrication methods of 2D materials including transition-metal dichalcogenides (TMDCs) and black phosphorus (BP).

LPE is another physical method that employs high-intensity ultrasound to generate microbubbles to continuously destroy the van der Waals forces between the layers [108, 109]. By selecting proper solvents or surfactant solutions, the LPE method can produce mass dispersions of mono-layer and few-layer nanosheets from pristine bulk material under ambient conditions. This method is quite simple and cost-effective, but can only produce small-size nanosheets and the layer number is difficult to precisely control.

CVD is a common approach for the synthesis of large-scale high-quality 2D materials [110, 111]. Generally, gaseous or pulverized reactants are sent to the reaction chamber under a high temperature to produce 2D materials on a substrate. Unlike the ME and LPE techniques, the defects and the layer number of 2D materials prepared by CVD can be controlled by reaction parameters. The CVD method is expected to be used for commercial productions, while the fabrication process is rather complicated and still requires further development. Unlike zero-bandgap graphene, few-layer Mo/WTe_2 and BP tend to be oxidized in air and need additional protection devices during fabrication and application.

2.2 Saturable absorption properties

Various nonlinear optical phenomena have been observed from 2D materials, such as high-order harmonic generation [112], four-wave mixing [113], and the Kerr effect [114]. Saturable absorption is a typical third-order nonlinear effect that the optical absorbance reduces with the increase of light intensity and becomes saturated at a certain threshold. Actually, the real part of third-order Kerr nonlinearity $\chi^{(3)}$ is related to the nonlinearity refractive index n_2 while the imaginary part of $\chi^{(3)}$ is responsible for the saturable absorption property.

SAs are frequently used in fiber lasers to generate passively Q-switched pulses or mode-locked pulses. The parameters of SAs include modulation depth (α_s), non-saturable loss (α_{ns}), and saturable intensity (I_{sat}). A broad operation bandwidth and high damage threshold are usually required for practical applications. The absorption coefficient $\alpha(I)$ and optical intensity I follow the equation [115]:

$$\alpha(I) = \alpha_{ns} + \frac{\alpha_s}{1 + I / I_{sat}}$$

The Z-scan technique is a common technique for characterizing the nonlinear absorption of materials [116–118]. The Z-scan setup is shown in Figure 2A, and is used to measure the intensity-dependent nonlinear susceptibility of materials. In the measurement arm, the sample is moved in the Z-direction along the axis of a focused laser beam and the far field intensity is measured as a function of the sample position. In the reference arm, detector 2 is used for monitoring the incident light intensity. The magnitude of the nonlinear index can be calculated from the dependence of the detector signal on the sample position.

The total absorption $\alpha(I) = \alpha_0 + \alpha_{NL} I$, where α_0 is the linear absorption coefficient, and nonlinear coefficient α_{NL} can be calculated by the data of the Z-scan curves based on the nonlinear propagation equation $dI/dz = -(\alpha_0 + \alpha_{NL} I)\, I$. The imaginary part of the third-order nonlinear optical susceptibility $\mathrm{Im}\chi^{(3)}$ is related to the nonlinear coefficient by $\mathrm{Im}\chi^{(3)} = [10^{-7} c\lambda n^2 / 96\pi^2]\alpha_{NL}$, where c is the speed of light in a vacuum, λ is the laser wavelength, and n is the refractive index [119]. The saturable intensity I_{sat} can be obtained from the equation of

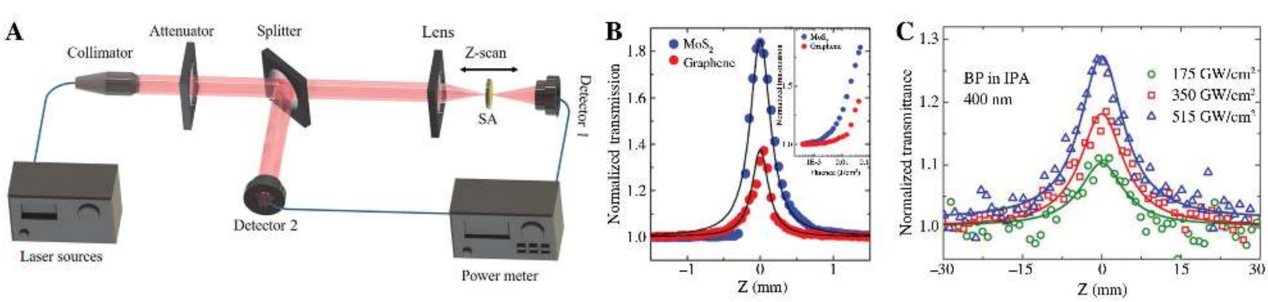

Figure 2: (A) Schematic of the Z-scan. (B) Comparison of nonlinear performance of MoS_2 (T = 34.4%) and graphene (T = 16.5%) dispersions, where MoS_2 shows a higher modulation depth. Inset: normalized transmission as a function of fluence. Reproduced with permission [116]. Copyright 2013, ACS Publishing. (C) Z-scan measurements of black phosphorus (BP) dispersions under different intensities at 400 nm. Reproduced with permission [76]. Copyright 2015, The Optical Society.

$dI/dz = -\alpha_0 I/(1+I/I_{sat})$, and the normalized transmittance can be expressed as [120–122]:

$$T(z) = \sum_{m=0}^{\infty} \left\{ \left[\frac{-\alpha(I) I_0 L_{eff}}{1+z^2/z_0^2} \right]^m \Big/ (m+1)^{3/2} \right\}$$

where $L_{eff} = (1-e^{-\alpha_0 L})/\alpha_0$, L is the sample length, I_0 is the on-axis peak intensity at the focus, z_0 is the Rayleigh diffraction length, and z is the longitudinal displacement of the sample.

The saturable absorption properties of TMDCs have been extensively studied by researchers in recent years [123–125]. Wang et al. [116] reported the ultrafast saturable absorption in MoS_2 dispersions produced by LPE under femtosecond laser excitation at 800 nm. It is shown that MoS_2 exhibits a higher saturable absorption than that of graphene under the same experimental conditions, as illustrated in Figure 2B. Zhang et al. [126] revealed the broadband saturable absorption property of few-layered MoS_2 nanosheets utilizing the open-aperture Z-scan technique, and further demonstrated the passively Q-switched and mode-locked fiber lasers at wavelengths of 1.06 μm, 1.55 μm and 2.1 μm using the MoS_2 SA [127]. The broadband saturable absorption properties of TMDCs may arise from the defect-induced decrease of the bandgap [37]. The layered TMDCs display features of high third-order susceptibility (~10^{-19} m^2/V^2), acceptable saturation intensity, and tunable bandgap by varying the layer numbers of the material. The layer-dependent absorption wavelength and broadband saturable absorption property enables them to be used in optoelectronic and photonic applications [126, 128, 129].

Due to its layer-dependent bandgap, similar to TMDCs, the nonlinear optical response of BP can be tuned over a broad range from visible to mid-infrared wavelengths [130].

BP nanosheets with a thickness of 52 nm (104 layers) were prepared by the ultrasonicated method, which has a bandgap of 0.357 eV, corresponding to a wavelength of 3.48 μm [131]. The broadband saturable absorption (400–2799 nm) has been demonstrated using BP nanosheets exfoliated by the LPE method [76, 132, 133], as shown in Figure 2C. The wavelength-dependent relaxation times of BP nanosheets were determined to be 360 fs to 1.36 ps with photon energies from 1.55 eV to 0.61 eV. In a comparative study with graphene, it was found that BP has a faster carrier relaxation in near-infrared and mid-infrared wavelengths [132]. Compared with graphene, the few-layer BP is less stable because the P atom can easily react with oxygen and water, resulting in its rapid degradation in air. Thus, long-term stability is a key parameter for BP SAs.

The nonlinear optical properties of TMDCs and BP measured by the Z-scan method are summarized in Table 1. TMDCs and BP materials are found to exhibit a normalized transmittance higher than 30%, and the saturation intensity ranges from tens of GW/cm² to several hundreds of GW/cm².

2.3 Incorporation methods

Several schemes based on mirrors or fibers have been proposed to actualize TMDCs and BP SAs. The first type of SA is prepared by spin-coating nanomaterials on mirrors or quartz, as shown in Figure 3A. Such an SA is mainly used in solid-state lasers, and requires a complex coupling system for fiber laser applications. The second SA is prepared by mixing the 2D material nanosheets with composite materials, such as polyvinyl alcohol (PVA) and polymethyl methacrylate. Then, the film-type SA is sandwiched between two fiber facets with a connector (Figure 3B). Although the sandwich structure can be easily incorporated with fiber lasers, the low damage threshold and poor stability limit its further applications in high-power pulsed fiber lasers. The third type of SA is based on a nonlinear interaction between nanomaterials and the evanescent field of D-shaped fibers (DSFs) and tapered fibers, as shown in Figure 3C and D. Due to the weak evanescent field and long interaction length, the laser-induced

Table 1: Summarization of nonlinear optical properties of transition-metal dichalcogenides (TMDCs) and black phosphorus (BP).

2D Mater.	Laser parameters	T (%)	I_s (GW/cm²)	α_0 (cm⁻¹)	α_{NL} (cm/GW)	Im$\chi^{(3)}$ (esu)	Ref.
MoS_2	800 nm, 1 KHz, 100 fs	32.6	381±346	11.22	$-(2.42\pm0.8)\times10^{-2}$	$-(1.38\pm0.45)\times10^{-14}$	[116]
$MoSe_2$	800 nm, 1 KHz, 100 fs	45.3	590±225	7.93	$-(2.54\pm0.6)\times10^{-2}$	$-(1.45\pm0.34)\times10^{-15}$	[134]
$MoTe_2$	800 nm, 1 KHz, 40 fs	86.3	217±11	1.47	$-(3.7\pm1.2)\times10^{-2}$	$-(2.13\pm0.66)\times10^{-15}$	[126]
BP	400 nm, 1 kHz, 100 fs	70.5	455.3±55	3.49	$-(1.62\pm0.28)\times10^{-2}$	–	[76]
BP	800 nm, 1 kHz, 100 fs	85.6	334.6±43	1.55	$-(6.17\pm0.19)\times10^{-3}$	–	[76]
BP	1330 nm, 50 kHz, fs	45.9±2.2	382±60	7.8±0.5	$-(1.9\pm0.3)\times10^{-2}$	$-(1.83\pm0.29)\times10^{-14}$	[132]
BP	1550 nm, 50 kHz, fs	59.1±0.1	398±163	5.3±0.1	$-(1.8\pm0.9)\times10^{-2}$	$-(1.98\pm0.95)\times10^{-14}$	[132]
BP	2100 nm, 50 kHz, fs	60.6±0.5	71.3±28.2	5±0.1	$-(5.7\pm1.4)\times10^{-2}$	$-(8.49\pm2.1)\times10^{-14}$	[132]

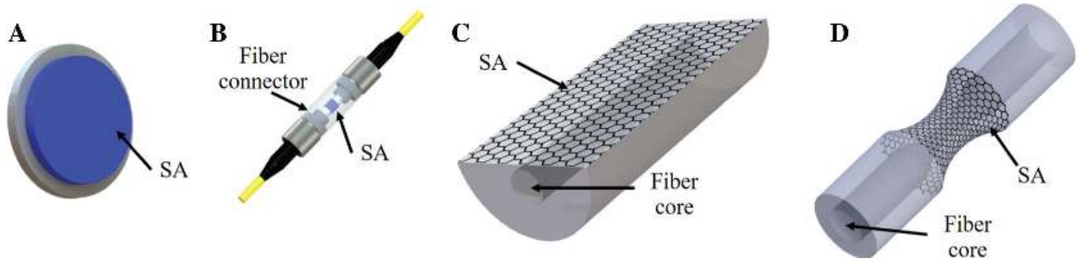

Figure 3: Incorporation methods.
(A) Spin coating 2D materials on mirrors or quartz. (B) Sandwiched structure. Transferring saturable absorber (SA) on (C) D-shaped fibers and (D) tapered fibers.

heating in DSFs and tapered fibers can be rapidly dispersed, and thus the SAs have a high damage threshold. However, the DSFs are polarization sensitive elements, and tapered fibers have a slight nonuniformity during the fabrication. When such components are inserted into the cavity, a nonlinear polarization rotation effect may occur and result in Q-switched or mode-locked operations.

Since graphene was first successfully applied as an SA, more and more 2D material-based SAs have been used in passively mode-locked and Q-switched fiber lasers. The broadband saturable absorption of TMDCs and BP enable them to be universal SAs for generating mode-locked and Q-switched pulses in ytterbium-doped fiber lasers (YDFLs), EDFLs, and thulium-doped fiber lasers, etc. In the following section, we discuss recent advances of pulsed fiber lasers at different wavelengths based on TMDCs and BP SAs.

3 Passively mode-locked fiber lasers based on TMDCs and BP SAs

3.1 Mode-locked fiber lasers at 1.06 µm

YDFLs usually work at 1.06 µm and have a large normal dispersion [135]. To realize the mode locking operation, the modulation depth of the SA must be large enough to compensate the dispersion-induced stretching of the pulse [28, 136]. Zhang et al. [129] demonstrated the first YDFL passively mode locked by an MoS_2 SA, and obtained 800 ps pulses at a wavelength of 1054 nm. The studies also revealed that the modulation depth of the MoS_2 SA is 10% at 400-nm excitation and 34% at 800-nm excitation, and the absorption wavelength spans from the visible band to the near-infrared band. Subsequently, we also realized dissipative soliton mode locking in an YDFL by using a WS_2-DSF SA, as illustrated in Figure 4A–C [137]. The modulation depth of the SA is about 2.9%, and the output pulse has a duration of 630 ps with a 3-dB spectral width of 0.77 nm. Single-pulse mode locking can be maintained at a pump power of 610 mW, and the maximum pulse energy is 13.6 nJ. It is demonstrated that the WS_2-DSF SA is capable of working at a high-power regime without damage. The strongly chirped dissipative solitons can be amplified external to the cavity to generate high-intensity pulses after compression. These progresses have greatly promoted the development of TMDC SAs and their applications in mode-locked fiber lasers at 1.06 µm [138, 139].

After that, few-layer BP has been prepared using the LPE method, and a fiber-based BP SA was achieved using the laser deposition method. With the proposed SA, Song et al. [140] reported dissipative soliton mode locking at 1030 nm in a YDFL, with a pulse duration of 400 ps and an output power of 32.5 mW. Hisyam et al. [141]

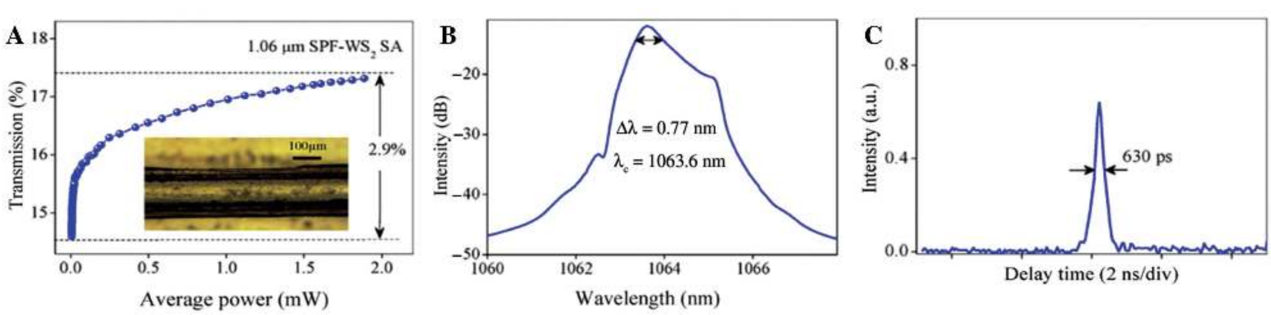

Figure 4: Mode-locked ytterbium-doped fiber lasers (YDFLs) based on WS_2-D-shaped fiber (DSF) saturable absorber (SA).
(A) Nonlinear transmission of the SA. (B) Spectrum. (C) Pulse profile. Reproduced with permission [137]. Copyright 2015, The Optical Society.

also reported a YDFL passively mode-locked by a BP SA, delivering an optical pulse train with a repetition rate of 13.5 MHz at a wavelength of 1085.58 nm. The maximum pulse energy is 5.93 nJ at a pump power of 1322 mW. The properties of mode-locked fiber lasers using TMDCs and BP SAs are summarized in Table 2. Although TMDCs and BP have much lower optical damage thresholds than that of graphene, the lateral interaction between the evanescent field and these 2D materials allows them to survive with a high incident power, which guarantees the reliable nonlinear effect against thermal damage for the dissipative soliton mode locking [26]. Based on TMDCs and BP SAs, dissipative solitons with a maximum pulse energy of 30 mW [139] and a shortest pulse duration of 7.54 ps [141] have been reported.

3.2 Mode-locked fiber lasers at 1.55 μm

EDFLs are the most important light source at 1.55 μm, and also provide a perfect platform to study the nonlinear properties of SAs. The fiber components are available from commercial optical communication systems, and it is easy to build all-fiber resonators without free-space bulk components. Xia et al. [142] achieved ultrafast pulses in an EDFL mode locked by a CVD-grown MoS_2 SA; the output pulses have a central wavelength, pulse duration, and repetition rate of 1568.9 nm, 1.28 ps, and 8.288 MHz, respectively. Zhang et al. [143] demonstrated a tunable mode-locked EDFL based on an MoS_2-PVA SA, in which the central wavelength is tunable from 1535 nm to 1565 nm. Similar to MoS_2, few-layer WS_2 also has remarkable saturable absorption properties and a high optical damage threshold [126]. Based on a WS_2-DSF SA, we have achieved soliton mode locking in an anomalous-dispersion EDFL [144] and dissipative soliton mode locking in a normal-dispersion EDFL [137]. A pulse with duration of 67 fs has also been reported in a mode-locked EDFL with the combination of fiber-taper WS_2 SA and the nonlinear polarization rotation technique [145].

With the assistance of the high-damage threshold SA, passively harmonic mode locking (HML) fiber lasers can also be obtained at the high pump regime. The principle of HML is that multiple pulses rearrange themselves in a regular position and the pulse repetition rate is the multiple of the fundamental repetition rate. By using an MoS_2-DSF SA, we have observed HML of bound-state pulses in an EDFL, as illustrated in Figure 5A–D. At a pump power of 600 mW, bound-state pulses with a separation of 3.4 ps are distributed equally in the cavity. The repetition rate of the bound-state pulses is 125 MHz, corresponding to 14th harmonic of fundamental cavity repetition rate [146]. Zhang et al. [147] also reported the 369th HML in an EDFL using a microfiber-based MoS_2 SA. A 2.5 GHz repetition rate pulse could be obtained at a pump power of 181 mW. So far, HML up to 3.25 GHz [148] and 3.27 GHz [149] has also been realized from EDFLs using WSe_2 and $MoSe_2$ SAs, respectively.

After that, many studies have demonstrated that other layered TMDCs and their derivatives including WSe_2 [148], $MoSe_2$ [150], WTe_2 [151], SnS_2 [138], ReS_2 [125] etc. could be used to prepare SAs for generating ultrafast mode-locked pulses in fiber lasers. We demonstrated soliton mode-locked fiber lasers utilizing two types of $MoTe_2$/WTe_2-based SAs, one of which is prepared by depositing the nanosheets on DSF, while the other is fabricated by mixing the nanosheets with PVA [152]. Yan et al. [104] achieved a mode-locked pulse with a duration of 229 fs and an average output power of 57 mW in an EDFL using a $MoTe_2$ SA that is fabricated by the magnetron sputtering deposition method.

In 2015, Zhang et al. [76] found that BP nanosheets have a saturable absorption property at 400 nm,

Table 2: Summarization of mode-locked fiber laser at 1.06 μm based transition-metal dichalcogenides (TMDCs) and black phosphorus (BP) saturable absorbers (SAs).

2D-Mater.	Fabrication method	Incorporation method	Laser performance				Ref.
			λ (nm)	Duration (ps)	Energy	RF (MHz)	
MoS_2	Hydrothermal exfoliation	DSF	1054.3	800	9.3 mW	7	[129]
WS_2	LPE	DSF	1063.6	630	13.6 nJ	5.57	[137]
WS_2	Thermal decomposition	Fluorine mica substrate	1052.45	288	30 mW	23.26	[139]
SnS_2	LPE	Sandwiched	1062.66	656	2.23 mW	39.33	[138]
BP	LPE	Sandwiched	1030.6	400	0.70 nJ	46.3	[140]
BP	ME	Sandwiched	1085.5	7.54	5.93 nJ	13.5	[141]

DSF, D-shaped fibers; LPE, liquid-phase exfoliation; ME, mechanical exfoliation; RF, repetition frequency.

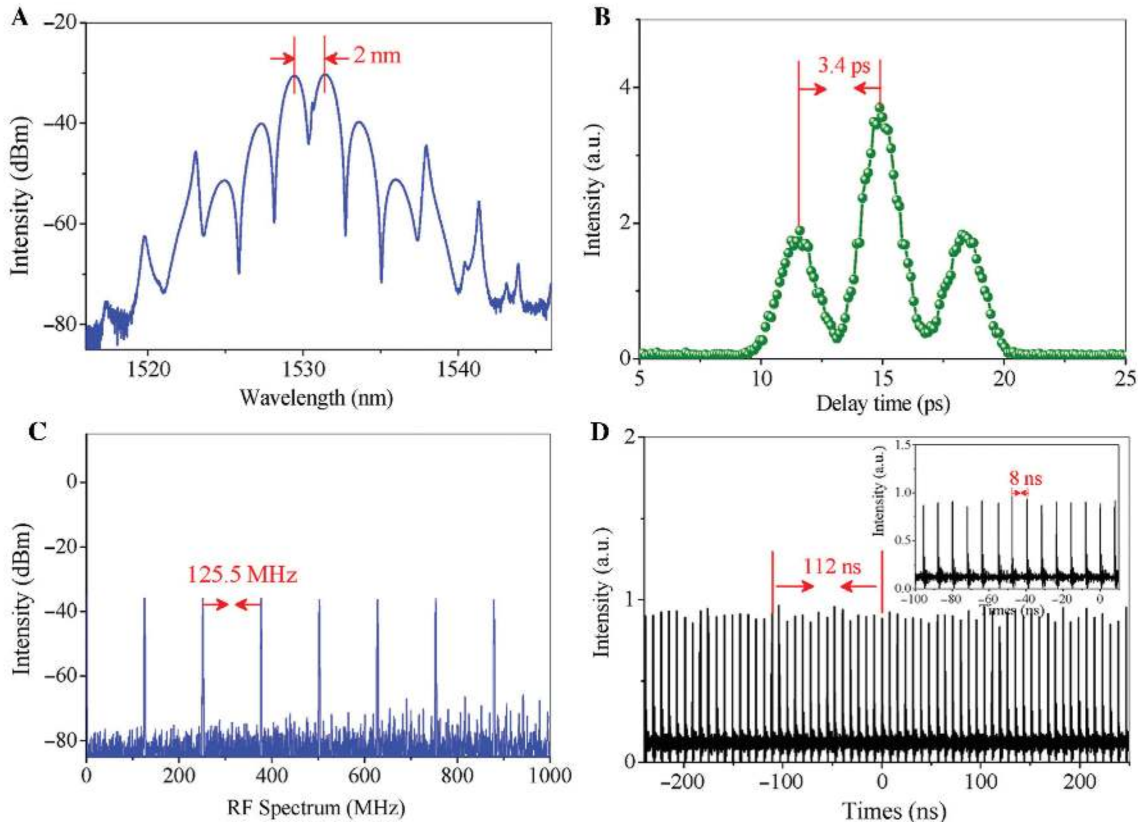

Figure 5: (A) Spectrum, (B) auto-correlation trace, (C) radiofrequency spectrum, and (D) oscilloscope trace of harmonic mode locking (HML) pulses based on MoS_2-D-shaped fiber (DSF) saturable absorber (SA).

800 nm, 1563 nm and 1930 nm using the Z-scan method. After that, various BP SAs have been fabricated and applied in fiber lasers to generate ultrafast pulses. Chen et al. [153] demonstrated a mode-locked EDFL by using the mechanically exfoliated BP as an SA, and obtained 946 fs transform limited pulses at a wavelength of 1571.45 nm, as depicted in Figure 6A–C. It is worth mentioning that Sotor et al. [74] and Sun et al. [155] reported that the mechanically exfoliated BP has a polarization-dependent absorption property, which is different from other 2D material SAs (i.e. graphene SAs, topological insulator SAs). The polarization-sensitive saturable absorption induces a polarization selection effect to the laser cavity and prevents the formation of the vector soliton. However, Zhang et al. [156] observed vector solitons in a mode-locked EDFL, in which the SA is based on BP nanosheets exfoliated by the LPE method. The generation of vector soliton can be understood by noting that BP nanosheets are distributed randomly in all orientations and the interaction area of the SA is much larger than the size of the nanosheets [157].

Various methods have been proposed to improve the stability of BP in air [158, 159]. For example, Jin et al. [154] demonstrated a self-starting mode-locking operation stable for >10 days without any noticeable performance degradation utilizing an inkjet-printed BP-SA, and obtained 102 fs pulses with 40 nm spectral width, as shown in Figure 6D–F. We have obtained anti-oxidized BP nanosheets based on the liquid exfoliation approach, using aqueous poly dimethyldiallyl ammonium chloride as a dispersion fluid. Based on the BP-polymer SA, passive mode-locking operations are realized in an EDFL, delivering a train of pulses with a duration of 1.2 ps at 1557.8 nm [160]. The properties of mode-locked EDFLs using TMDCs and BP SAs are summarized in Table 3. Up to now, to our knowledge, the shortest pulse duration of 67 fs has been achieved in an EDFL with the combination of the fiber-taper WS_2 SA and the nonlinear polarization rotation technique [145], the highest pulse repetition rate (3.27 GHz) has been reported by using an $MoSe_2$ SA in the HML [149], and the maximum output power of 57 mW has been obtained by using the $MoTe_2$ SA prepared by the magnetron-sputtering deposition method [104].

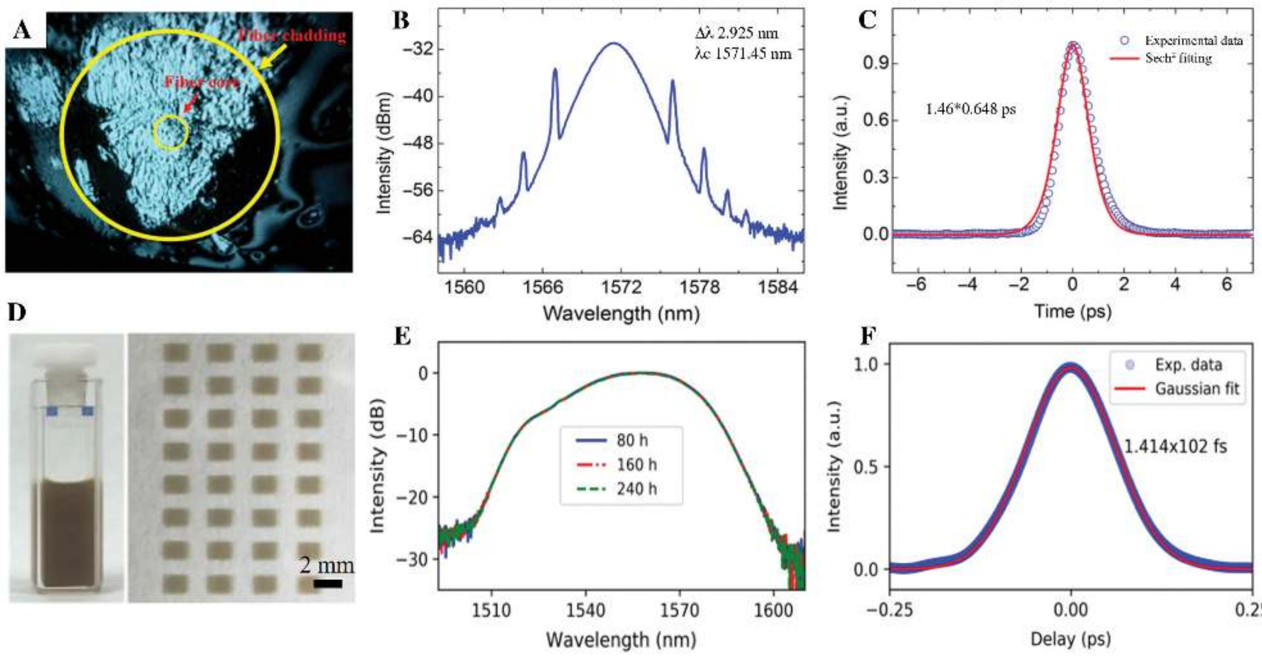

Figure 6: Typical mode-locked erbium-doped fiber lasers (EDFLs) by black phosphorus (BP) saturable absorbers (SAs). (A) Optical image of BP on fiber facet. (B) Pulse spectrum. (C) Autocorrelation traces. Reproduced with permission [153]. Copyright 2015, The Optical Society. (D) Photograph of BP dispersion and inkjet-printed BP SA arrays. (E) Spectra of mode-locked pulse acquired after 80 h, 160 h and 240 h. (F) Autocorrelation traces. Reproduced with permission [154]. Copyright 2018, The Optical Society.

Table 3: Summarization of mode-locked erbium-doped fiber lasers (EDFLs) based on transition-metal dichalcogenides (TMDCs) and black phosphorus (BP) saturable absorbers (SAs) at 1.55 μm.

2D-Mater.	Fabrication method	Incorporation method	Laser performance				Ref.
			λ (nm)	Duration (fs)	Energy	RF (MHz)	
MoS_2	CVD	Sandwiched	1568.9	1280	–	8.288	[142]
MoS_2	LPE	PVA film	1535–1565	ps	65 pJ	12.99	[143]
WS_2	LPE	PVA-film	1557	1320	0.248 nJ	8.86	[144]
WS_2	PLD	Tapered fiber	1540	67	–	135	[145]
MoS_2	LPE	DSF	1530.4	1210	–	125	[146]
MoS_2	LPE	DSF	1556.86	3000	–	2.5 GHz	[147]
MoS_2	CVD	DSF	1568	4980	–	26.02	[161]
MoS_2	LPE	PVA film	1569.5	710	22 mW	12.09	[162]
WS_2	Solution	DSF	1557	660	–	10.2	[163]
WS_2	LPE	Tapered fiber	1561	369	1.93 mW	24.93	[164]
WS_2	PLD	Tapered fiber	1561	246	18 mW	101.4	[165]
$MoTe_2$	MSD	Tapered fiber	1559.57	229	57 mW	26.601	[104]
$MoSe_2$	CVD	Tapered fiber	1552	207	–	64.56	[150]
WTe_2	LPE	DSF	1556.2	770	–	13.98	[151]
SnS_2	LPE	PVA film	1562.01	623	1.2 mW	29.33	[138]
ReS_2	LPE	PVA film	1558.6	1600	0.4 mW	5.48	[125]
BP	ME	Sandwiched	1571.45	946	–	5.96	[153]
BP	ME	Sandwiched	1559.5	670	–	8.77	[156]
BP	ME	Sandwiched	1558.7	786	0.11 nJ	14.7	[155]
BP	LPE	Sandwiched	1555	102	0.071 nJ	23.9	[154]
BP	LPE	PVA film	1557.8	1200	–	6.317	[160]
BP	ME	Sandwiched	1560.5	946	–	5.96	[153]

CVD, chemical vapor deposition; DSF, D-shaped fibers; LPE, liquid-phase exfoliation; ME, mechanical exfoliation; MSD, magnetron sputtering deposition; PLD, pulsed laser deposition; RF, repetition frequency; PVA, polyvinyl alcohol.

3.3 Mode-locked fiber lasers at mid-infrared wavelengths

Ultrafast fiber lasers operating from 2 μm to 20 μm wavelength are one of the most important branches of laser technology [166–169]. Mid-infrared fiber lasers are experiencing intense development due to their important applications in remote sensing [170], spectroscopy [171, 172], environmental monitoring [173, 174], materials processing [175], etc. In the mid-infrared region, the study of ultrafast fiber lasers started in the 1990s since Nelson et al. [176] demonstrated a mode-locked Tm^{3+}-doped fiber laser that produced sub-500 fs pulses. After that, ultrafast fiber lasers developed rapidly in this waveband, and a number of mode-locked Tm^{3+}-, Ho^{3+}-, and Ho^{3+}/Pr^{3+}-doped fiber lasers have been reported [177–180]. Simultaneously, the booming advances of low-dimensional nanomaterials over the past decade have triggered an increasing interest in nanomaterial-based SAs at mid-infrared wavelengths [181–184]. Up to now, 2 μm mode-locked fiber lasers have been achieved with the assistance of layered materials. In 2017, Jung et al. [185] reported mode locking in Tm^{3+}/Ho^{3+} co-doped fiber lasers by a WS_2-DSF SA, and achieved stable mode-locked pulses with a width of ~1.3 ps at a repetition rate of 34.8 MHz at 1941 nm, as shown in Figure 7A–C.

Stimulated by the applications in atmospheric remote sensing [187], the wavelengths of fiber lasers have been extended beyond the 3 μm regime. However, TMDCs such as MoS_2 and WS_2 generally have large bandgaps (1~2 eV), which limits their applications in the mid-infrared wavelength >3 μm. Depending on the number of layers [23], BP has a tunable direct energy bandgap from 0.3 eV to 2 eV, which makes it an ideal saturable absorption material, especially in the mid-infrared wavelength region.

The first BP mode-locked operation at 3 μm was reported by Li et al. [188] in an Ho^{3+}/Pr^{3+} co-doped fluoride fiber laser, where BP was fabricated using the LPE method and then integrated with a mirror. The pulse duration, repetition rate, and output power are 8.6 ps, 13.987 MHz, and 6.28 nJ, respectively. Qin et al. reported a passively mode-locked Er: ZBLAN fiber laser by transferring the thickness of ~143 nm BP nanosheets onto the gold-coated mirror to serve as a BP SA. The mode-locked mid-infrared laser at 2783 nm generated a pulse with an average output power of 613 mW, a pulse duration of 42 ps and a repetition rate of 24 MHz, as shown in Figure 7D and E [186]. Qin et al. [131] reported a mode-locked Er-doped ZBLAN fiber laser at 3.48 μm by transferring 52 nm BP flakes onto an Au-coated mirror as the SA, producing picosecond pulses with an average power of 40 mW and a repetition rate of

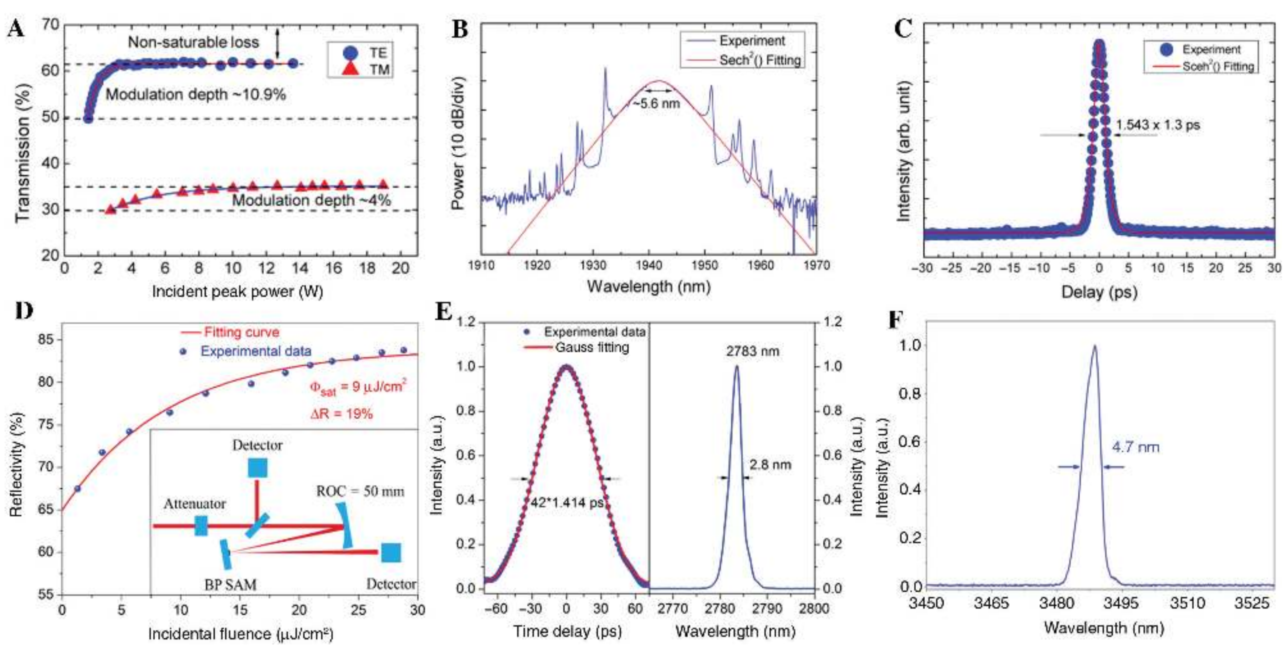

Figure 7: Mode-locked fiber lasers using WS_2 saturable absorber (SA).
(A) Nonlinear transmission curves at 1925 nm. (B) Spectrum. (C) Autocorrelation traces. Reproduced with permission [185]. Copyright 2015, The Optical Society. Mode-locked Er: ZBLAN fiber laser at 2.8 μm and 3.5 μm. (D) Saturable absorption of black phosphorus (BP) SA at 2.8 μm. (E) Autocorrelation trace and spectrum at 2.8 μm. Reproduced with permission [186]. Copyright 2016, The Optical Society. (F) Spectrum at 3.5 μm. Reproduced with permission [131]. Copyright 2018, The Optical Society.

Table 4: Summarization of mode-locked fiber lasers with transition-metal dichalcogenides (TMDCs) and black phosphorus (BP) saturable absorbers (SAs) at mid-infrared wavelengths.

2D-Mater.	Fabrication method	Incorporation method	Laser performance					Ref.
			Laser type	λ (nm)	Duration (ps)	Energy	RF(MHz)	
WS_2	LPE	DSF	Tm/Ho	1941	1.3	17.2 pJ	34.8	[185]
$MoSe_2$	LPE	DSF	Tm/Ho	1912	920	4.3 mW	18.21	[190]
WTe_2	MSD	Microfiber	Tm	1915.5	1.25	39.9 mW	18.72	[189]
BP	ME	Fiber end facet	Tm	1910	739	0.047 nJ	36.8	[74]
BP	LPE	SA mirror	Ho^{3+}/Pr^{3+}	2866.7	8.6	6.28 nJ	13.987	[188]
BP	ME	SA mirror	Er: ZBLAN	2783	42	613 mW	24	[186]
BP	Sonication	SA mirror	Er: ZBLAN	3489	–	40 mW	28.91	[131]

DSF, D-shaped fibers; LPE, liquid-phase exfoliation; ME, mechanical exfoliation; MSD, magnetron sputtering deposition; RF, repetition frequency.

28.91 MHz, as illustrated in Figure 7F. Besides the BP SA, by introducing defects in MoS_2 [180], WS_2 [185], WTe_2 [189], $MoSe_2$ [190], mode-locked Tm^{3+}-, Ho^{3+}-, Ho^{3+}/Pr^{3+}, ZBLAN-doped fiber lasers have been reported using TMDC SAs. Table 4 summarizes these important achievements of mode-locked fiber lasers with TMDCs and BP SAs at mid-infrared wavelengths.

4 Passively Q-switched fiber lasers based on TMDCs and BP SAs

Passive Q-switching is another important technique for generating pulsed lasers, which have nanosecond/microsecond pulse duration and a large pulse energy at the kHz repetition rate [191]. Attributed to their remarkable high pulse energy, Q-switched fiber lasers can be applied in many fields, such as industrial laser engraving, metal cutting, and laser surgery. Compared with mode-locked fiber lasers that require a careful design of the cavity to balance the dispersion and nonlinearity, Q-switched fiber lasers are quite easy for implementation by modulating the loss of a laser oscillator. An SESAM was generally used to achieve passively Q-switched operation in previous commercial laser systems. However, the fabrication of an SESAM usually requires expensive and complicated fabrication systems and the SAs have bandwidths less than 50 nm. Thus, a low-cost high-performance Q-switcher is quite urgent for practical applications. Benefiting from the broadband property of TMDCs and BP SAs, the wavelength of passively Q-switched fiber lasers can range from the visible to mid-infrared range [192–197].

Li et al. [198] have generated 604 nm Q-switched pulses in Pr^{3+}-doped fiber lasers utilizing filmy WS_2 and MoS_2 SA. For WS_2 (MoS_2) SAs, the pulse has a repetition rate of 67.3~132.2 kHz (50.8~118.4 kHz) with a minimum duration of 435 ns (602 ns). Woodward et al. [199] have demonstrated a passively Q-switched YDFL tunable from 1030 nm to 1070 nm based on an MoS_2-PVA SA. Luo et al. [200] also demonstrated passively Q-switched fiber lasers at 1 μm, 1.5 μm, and 2 μm by exploiting a few-layer MoS_2-polymer SA. Jiang et al. [201] achieved a passively Q-switched thulium/holmium-doped fiber laser at 2 μm by a BP-SA that is fabricated by the optical deposition method. The Q-switched pulse has a minimum duration of ~731 ns, a maximum pulse energy of 632.4 nJ, and a repetition rate of 69.4 ~ 113.3 kHz. Qin et al. [131] reported a Q-switched Er: ZBLAN fiber laser at 3462 nm by transferring BP flakes onto an Au-coated mirror. The output power, pulse width, and repetition rate are 120 mW, 2.05 μs, and 66.33 kHz, respectively. Table 5 summarizes these important progresses of Q-switched fiber lasers based on TMDCs and BP SAs.

5 Summary and outlook

TMDCs and BP are two typical layered 2D nanomaterials that have a large third-order nonlinearity and layer-dependent bandgap. In this review, we have discussed nonlinear optical properties and fabrication methods of TMDCs and BP nanosheets, and summarized typical approaches of incorporating nanosheets with fibers to achieve fiber-based SAs. In the main part, we have also highlighted the recent progresses of mode-locked and Q-switched fiber lasers from the visible to mid-infrared regime. The pure TMDCs exhibit comparatively large bandgaps in the visible or near-infrared wavelength region (~1.8 eV for MoS_2, ~2.1 eV for WS_2, ~0.8 eV for WTe_2). Although their bandgaps can be controlled by changing the layer numbers or introducing atomic defects, the

Table 5: Summarization of Q-switched fiber lasers based on transition-metal dichalcogenides (TMDCs) and black phosphorus (BP) saturable absorbers (SAs).

2D-Mater.	Fabrication method	Incorporation method	Laser performance					Ref.
			Laser type	λ (nm)	Duration	Energy	RF (KHz)	
MoS_2	LPE	SA mirror	Pr^{3+} ZBLAN	604	602 ns	5.5 nJ	50.8–118.4	[198]
MoS_2	LPE	Sandwiched	Yb	1030–1070	2.88 μs	126 nJ	65.3–89	[199]
MoS_2	Hydrothermal	PVA	Er	1560	3.2–5.1 μs	17.16 nJ	36.8–91.7	[202]
MoS_2	Thermal evaporation	Sandwiched	Er	1550–1575	6–35 μs	150 nJ	22	[203]
MoS_2	CVD	Sandwiched	Er	1529.8–1570.1	1.92 μs	8.2 nJ	28.6–114.8	[204]
MoS_2	LPE	Sandwiched	Er	1519.6–1567.7	3.3 μs	160 nJ	8.77–43.47	[205]
MoS_2	PLD	SA mirror	Er	1549.8	660 ns	152 nJ	116–131	[206]
MoS_2	LPE	Sandwiched	Tm	2030	1.76 μs	1 μJ	33.6–48.1	[200]
WS_2	LPE	SA mirror	Pr^{3+} ZBLAN	604	435 ns	6.4 nJ	67.3–132.2	[198]
WS_2	CVD	PVA	Yb	1027–1065	1.65 μs	–	60.2–97	[207]
WS_2	LPE	Sandwiched	Er	1547.5	985 ns	44 nJ	80–120	[208]
WS_2	LPE	Sandwiched	Er	1550	4.04 μs	369.5 nJ	60.724–66.847	[197]
$MoSe_2$	LPE	Sandwiched	Tm	1924	5.5 μs	42 nJ	14–21.8	[209]
$TiSe_2$	PMS/CVD	SA mirror	Er	1530	1.126 μs	11.5 mW	70–154	[210]
BP	LPE	Sandwiched	Pr^{3+} ZBLAN	635	383–1560 ns	27.6 nJ	108.8–409.8	[211]
BP	ME	Microfiber	Yb	1064.7	2.0–5.5 μs	17.8 nJ	26–76	[212]
BP	ME	Sandwiched	Er	1561.9	2.96 μs	194 nJ	7.86–34.32	[213]
BP	Solution	Sandwiched	Tm/Ho	1912	731 μs	632.4 nJ	69.4–113.3	[201]
BP	LPE	SA mirror	Er: ZBLAN	2800	1.18–2.1 μs	7.7 μJ	39–63	[214]
BP	Sonication	SA mirror	Er: ZBLAN	3462	2.05 μs	1.83 μJ	66.33	[131]

CVD, chemical vapor deposition; LPE, liquid-phase exfoliation; ME, mechanical exfoliation; PLD, pulsed laser deposition; PMS, pulse magnetron sputtering; PVA, polyvinyl alcohol; RF, repetition frequency.

absorption is relatively weak in the mid-infrared wavelength. Thus, the TMDC-based SAs are difficult to apply in mid-infrared lasers. In contrast to TMDCs, the bandgap of BP can be tuned from 0.3 eV to 2 eV (corresponding to the wavelength from 4 μm to 0.6 μm) depending on the layer number. Thus, BP SAs are more attractive for pulsed fiber lasers at mid-infrared wavelengths.

In addition to their widespread applications in fiber lasers [65, 215], these 2D materials have also been used as SAs to realize mode-locked/Q-switched operations in solid-state lasers [216, 217] and waveguide lasers [218, 219] from visible to mid-infrared wavelengths. Although many breakthroughs of these studies have been achieved in recent years, there are still many challenges. For instance, the high nonsaturable loss of 2D material SAs limits the efficiency of fiber lasers. The pulsed fiber laser based on the TMDCs and BP SAs can be further optimized by changing the cavity design and growing high-quality 2D materials. Fiber lasers can be further extended to shorter or longer wavelengths using new fibers and a gain medium. More importantly, how to transfer the laboratory technology for commercial applications is the key direction in the future.

For perspective, the TMDCs and BP SAs can be further developed from several aspects, such as reducing the nonsaturable loss, improving the stability, and controlling the modulation depth. With the development of mid-infrared fiber components, we expect that BP can be used as an SA in mid-infrared fiber lasers beyond 4 μm. Moreover, TMDCs and BP SAs can be used in few-mode fiber lasers or multi-mode fiber lasers to generate spatial-temporal mode-locked pulses [135]. The growing interest of exploring TMDCs and BP encourages researchers to look for new physics and technology breakthroughs, and also further exploit practical applications, including not only SAs, but also photodetectors, optical modulators and light-emitting devices.

Acknowledgements: This work was supported by the National Key R&D Program of China (2017YFA0303800); National Natural Science Foundation of China (11874300, Funder Id: http://dx.doi.org/10.13039/501100001809, 61575162); the Fundamental Research Funds for the Central Universities (3102017AX009, 3102019PY002, 3102019JC008); the Natural Science Foundation of Shannxi Province (2018JM6013).

References

[1] Liang C, Lee KF, Levin T, Chen J, Kumar P. Ultra stable all-fiber telecom-band entangled photon-pair source for turnkey quantum communication applications. Opt Express 2006;14:6936–41.

[2] Li Z, Heidt AM, Daniel JMO, Jung Y, Alam SU, Richardson DJ. Thulium-doped fiber amplifier for optical communications at 2 μm. Opt Express 2013;21:9289–97.

[3] Xu C, Wise FW. Recent advances in fiber lasers for nonlinear microscopy. Nat Photonics 2013;7:875–82.

[4] Pierce MC, Jackson SD, Golding PS, et al. Development and application of fiber lasers for medical applications. Optical Fibers and Sensors for Medical Applications 2001;4253:144–54.

[5] Gattass RR, Mazur E. Femtosecond laser micromachining in transparent materials. Nat Photonics 2008;2:219–25.

[6] Presby HM, Benner A, Edwards C. Laser micromachining of efficient fiber microlenses. Appl Optics 1990;29:2692–5.

[7] Keller U, Weingarten KJ, Kartner FX, et al. Semiconductor saturable absorber mirrors (SESAM's) for femtosecond to nanosecond pulse generation in solid-state lasers. IEEE J Sel Top Quant Electr 1996;2:435–53.

[8] Schriber C, Emaury F, Diebold A, et al. Dual-gain SESAM mode-locked thin disk laser based on Yb: Lu_2O_3 and Yb: Sc_2O_3. Opt Express 2014;22:18979–86.

[9] Krzempek K, Sobon G, Kaczmarek P, Abramski KM. A sub-100 fs stretched-pulse 205 MHz repetition rate passively mode-locked Er-doped all-fiber laser. Laser Phys Lett 2013;10:105103.

[10] Yun L, Han DD. Evolution of dual-wavelength fiber laser from continuous wave to soliton pulses. Opt Commun 2012;285:5406–9.

[11] Liu X, Si J, Chang B, et al. Third-order optical nonlinearity of the carbon nanotubes. Appl Phys Lett 1999;74:164.

[12] Cui Y, Liu X. Graphene and nanotube mode-locked fiber laser emitting dissipative and conventional solitons. Opt Express 2013;21:18969–74.

[13] Doran NJ, Wood D. Nonlinear-optical loop mirror. Opt Lett 1988;13:56–8.

[14] Ilday F, Wise F, Sosnowski T. High-energy femtosecond stretched-pulse fiber laser with a nonlinear optical loop mirror. Opt Lett 2002;27:1531–3.

[15] Autere A, Jussila H, Dai Y, Wang Y, Lipsanen H, Sun Z. Nonlinear optics with 2D layered materials. Adv Mater 2018;30:e1705963.

[16] Zhang W, Wang Q, Chen Y, Wang Z, Wee AT. Van der Waals stacked 2D layered materials for optoelectronics. 2D Mater 2016;3:022001.

[17] Xie Z, Xing C, Huang W, et al. Ultrathin 2D nonlayered tellurium nanosheets: facile liquid-phase exfoliation, characterization, and photoresponse with high performance and enhanced stability. Adv Funct Mater 2018;28:1705833.

[18] Xing C, Xie Z, Liang Z, et al. 2D nonlayered selenium nanosheets: facile synthesis, photoluminescence, and ultrafast photonics. Adv Opt Mater 2017;5:1700884.

[19] Huang W, Xie Z, Fan T, et al. Black-phosphorus-analogue tin monosulfide: an emerging optoelectronic two-dimensional material for high-performance photodetection with improved stability under ambient/harsh conditions. J Mater Chem C 2018;6:9582–93.

[20] Fan T, Xie Z, Huang W, Li Z, Zhang H. Two-dimensional non-layered selenium nanoflakes: Facile fabrications and applications for self-powered photo-detector. Nanotechnology 2019;30:114002.

[21] Xing C, Huang W, Xie Z, et al. Ultrasmall bismuth quantum dots: facile liquid-phase exfoliation, characterization, and application in high-performance UV–Vis photodetector. ACS Photonics 2018;5:621–9.

[22] Xie Z, Wang D, Fan T, et al. Black phosphorus analogue tin sulfide nanosheets: synthesis and application as near-infrared photothermal agents and drug delivery platforms for cancer therapy. J Mater Chem B 2018;6:4747–55.

[23] Xie Z, Chen S, Duo Y, et al. Biocompatible two-dimensional titanium nanosheets for multimodal imaging-guided cancer theranostics. ACS Appl Mater Inter 2019;11:22129–40.

[24] Liang X, Ye X, Wang C, et al. Photothermal cancer immunotherapy by erythrocyte membrane-coated black phosphorus formulation. J Controlled Release 2019;296:150–61.

[25] Pomerantseva E, Gogotsi Y. Two-dimensional heterostructures for energy storage. Nat Energy 2017;2:17089.

[26] Dong Y, Wu Z-S, Ren W, Cheng H-M, Bao X. Graphene: a promising 2D material for electrochemical energy storage. Sci Bull 2017;62:724–40.

[27] Xie Z, Peng YP, Yu L, et al. Solar-inspired water purification based on emerging two-dimensional materials: status and challenges. J Solar RRL 2020;1900400:1–28.

[28] Woodward RI, Kelleher EJ. 2D saturable absorbers for fibre lasers. Appl Sci 2015;5:1440–56.

[29] Guo B, Xiao QL, Wang SH, Zhang H. 2D layered materials: synthesis, nonlinear optical properties, and device applications. Laser Photon Rev 2019;13:1800327.

[30] Novoselov KS, Geim AK, Morozov SV, et al. Electric field effect in atomically thin carbon films. Science 2004;306:666–9.

[31] Bao Q, Zhang H, Wang Y, et al. Atomic-layer graphene as a saturable absorber for ultrafast pulsed lasers. Adv Funct Mater 2009;19:3077–83.

[32] Hasan T, Sun Z, Wang F, et al. Nanotube-polymer composites for ultrafast photonics. Adv Mater 2009;21:3874–99.

[33] Sun Z, Hasan T, Ferrari AC. Ultrafast lasers mode-locked by nanotubes and graphene. Phys E (Amsterdam, Neth) 2012;44:1082–91.

[34] Li X, Tang Y, Yan Z, et al. Broadband saturable absorption of graphene oxide thin film and its application in pulsed fiber lasers. IEEE J Sel Top Quantum Electron 2014;20:1101107.

[35] Zhang H, Tang D, Zhao L, Bao Q, Loh K. Large energy mode locking of an erbium-doped fiber laser with atomic layer graphene. Opt Express 2009;17:17630–5.

[36] Zhang H, Liu CX, Qi XL, Dai X, Fang Z, Zhang SC. Topological insulators in Bi_2Se_3, Bi_2Te_3 and Sb_2Te_3 with a single Dirac cone on the surface. Nat Phys 2009;5:438.

[37] Yu H, Zhang H, Wang Y, et al. Topological insulator as an optical modulator for pulsed solid-state lasers. Laser Photon Rev 2013;7:L77–L83.

[38] Xia Y, Qian D, Hsieh D, et al. Observation of a large-gap topological-insulator class with a single Dirac cone on the surface. Nat Phys 2009;5:398.

[39] Yan P, Lin R, Ruan S, et al. A practical topological insulator saturable absorber for mode-locked fiber laser. Sci Rep 2015;5:8690.

[40] Luo Z, Huang Y, Weng J, et al. 1.06 mum Q-switched ytterbium-doped fiber laser using few-layer topological insulator Bi_2Se_3 as a saturable absorber. Opt Express 2013;21:29516–22.

[41] Chi C, Lee J, Koo J, Han Lee J. All-normal-dispersion dissipative-soliton fiber laser at 1.06 μm using a bulk-structured Bi_2Te_3 topological insulator-deposited side-polished fiber. Laser Phys 2014;24:105106.

[42] Liu W, Pang L, Han H, et al. 70-fs mode-locked erbium-doped fiber laser with topological insulator. Sci Rep 2016;6:19997.
[43] Yu Z, Song Y, Tian J, et al. High-repetition-rate Q-switched fiber laser with high quality topological insulator Bi_2Se_3 film. Opt Express 2014;22:11508–15.
[44] Luo Z, Liu C, Huang Y, et al. Topological-insulator passively Q-switched double-clad Fiber laser at 2 μm wavelength. IEEE J Sel Top Quantum Electron 2014;20:1–8.
[45] Jung M, Lee J, Koo J, et al. A femtosecond pulse fiber laser at 1935 nm using a bulk-structured Bi_2Te_3 topological insulator. Opt Express 2014;22:7865–74.
[46] Wang QH, Kalantar Zadeh K, Kis A, Coleman JN, Strano MS. Electronics and optoelectronics of two-dimensional transition metal dichalcogenides. Nat Nanotechnol 2012;7:699.
[47] Chhowalla M, Shin HS, Eda G, Li LJ, Loh KP, Zhang H. The chemistry of two-dimensional layered transition metal dichalcogenide nanosheets. Nat Chem 2013;5:263.
[48] Manzeli S, Ovchinnikov D, Pasquier D, Yazyev OV, Kis A. 2D transition metal dichalcogenides. Nat Rev Mater 2017;2:17033.
[49] Mak KF, Shan J. Photonics and optoelectronics of 2D semiconductor transition metal dichalcogenides. Nat Photon 2016;10:216.
[50] Hsu WT, Zhao ZA, Li LJ, et al. Second harmonic generation from artificially stacked transition metal dichalcogenide twisted bilayers. ACS Nano 2014;8:2951–8.
[51] Seyler KL, Schaibley JR, Gong P, et al. Electrical control of second-harmonic generation in a WSe_2 monolayer transistor. Nat Nanotechnol 2015;10:407–11.
[52] Zhao G, Han S, Wang A, et al. “Chemical weathering” exfoliation of atom-thick transition metal dichalcogenides and their ultrafast saturable absorption properties. Adv Funct Mater 2015;25:5292–9.
[53] Bikorimana S, Lama P, Walser A, et al. Nonlinear optical responses in two-dimensional transition metal dichalcogenide multilayer: WS_2, WSe_2, MoS_2 and $Mo_{0.5}W_{0.5}S_2$. Opt Express 2016;24:20685–95.
[54] Chen H, Yin J, Yang J, et al. Transition-metal dichalcogenides heterostructure saturable absorbers for ultrafast photonics. Opt Lett 2017;42:4279–82.
[55] Zeng H, Cui X. An optical spectroscopic study on two-dimensional group-VI transition metal dichalcogenides. Chem Soc Rev 2015;44:2629–42.
[56] Dong N, Li Y, Zhang S, et al. Saturation of two-photon absorption in layered transition metal dichalcogenides: experiment and theory. ACS Photonics 2018;5:1558–65.
[57] Kumar A, Ahluwalia PK. Electronic structure of transition metal dichalcogenides monolayers 1H-MX_2 (M = Mo, W; X = S, Se, Te) from ab-initio theory: new direct band gap semiconductors. Eur Phys J B 2012;85:186.
[58] Ugeda MM, Bradley AJ, Shi S-F, et al. Giant bandgap renormalization and excitonic effects in a monolayer transition metal dichalcogenide semiconductor. Nat Mater 2014;13:1091–5.
[59] Chen Y, Xi J, Dumcenco DO, et al. Tunable band gap photoluminescence from atomically thin transition-metal dichalcogenide alloys. Acs Nano 2013;7:4610–6.
[60] Kuc A, Zibouche N, Heine T. Influence of quantum confinement on the electronic structure of the transition metal sulfide TS_2. Phys Rev B 2011;83:245213.
[61] Guo S, Zhang Y, Ge Y, Zhang S, Zeng H, Zhang H. 2D V-V binary materials: status and challenges. Adv Mater 2019;31:1902352.
[62] Zhang S, Yan Z, Li Y, Chen Z, Zeng H. Atomically thin arsenene and antimonene: semimetal-semiconductor and indirect-direct band-gap transitions. Angew Chem 2015;54:3112–5.
[63] Lu L, Tang X, Cao R, et al. Broadband nonlinear optical response in few-layer antimonene and antimonene quantum dots: a promising optical Kerr media with enhanced stability. Adv Opt Mater 2017;5:1700301.
[64] Lu L, Liang Z, Wu L, et al. Few-layer bismuthene: sonochemical exfoliation, nonlinear optics and applications for ultrafast photonics with enhanced stability. Laser Photon Rev 2018;12:1700221.
[65] Zhang M, Wu Q, Zhang F, et al. 2D black phosphorus saturable absorbers for ultrafast photonics. Adv Opt Mater 2019;7:1800224.
[66] Wang X, Lan S. Optical properties of black phosphorus. Adv Opt Photon 2016;8:618–55.
[67] Xia F, Wang H, Jia Y. Rediscovering black phosphorus as an anisotropic layered material for optoelectronics and electronics. Nat Commun 2014;5:4458.
[68] Huang M, Wang M, Chen C, et al. Broadband black-phosphorus photodetectors with high responsivity. Adv Mater 2016;28:3481–5.
[69] Guo Z, Zhang H, Lu S, et al. From black phosphorus to phosphorene: basic solvent exfoliation, evolution of Raman scattering, and applications to ultrafast photonics. Adv Funct Mater 2015;25:6996–7002.
[70] Li L, Kim J, Jin C, et al. Direct observation of the layer-dependent electronic structure in phosphorene. Nat Nanotechnol 2017;12:21.
[71] Lei W, Zhang T, Liu P, Rodriguez JA, Liu G, Liu M. Bandgap-and local field-dependent photoactivity of Ag/black phosphorus nanohybrids. ACS Catal 2016;6:8009–20.
[72] Liu Y, Duan X, Huang Y, Duan X. Two-dimensional transistors beyond graphene and TMDCs. Chem Soc Rev 2018;47:6388–409.
[73] Wang Y, Huang G, Mu H, et al. Ultrafast recovery time and broadband saturable absorption properties of black phosphorus suspension. Appl Phys Lett 2015;107:091905.
[74] Sotor J, Sobon G, Macherzynski W, Paletko P, Abramski KM. Black phosphorus saturable absorber for ultrashort pulse generation. Appl Phys Lett 2015;107:051108.
[75] Mao D, Li M, Cui X, et al. Stable high-power saturable absorber based on polymer-black-phosphorus films. Opt Commun 2018;406:254–9.
[76] Lu SB, Miao LL, Guo ZN, et al. Broadband nonlinear optical response in multi-layer black phosphorus: an emerging infrared and mid-infrared optical material. Opt Express 2015;23:11183–94.
[77] Lin C, Grassi R, Low T, Helmy AS. Multilayer black phosphorus as a versatile mid-infrared electro-optic material. Nano Lett 2016;16:1683–9.
[78] Song Y, Shi X, Wu C, Tang D, Zhang H. Recent progress of study on optical solitons in fiber lasers. Appl Phys Rev 2019;6:021313.
[79] Xie Z, Zhang F, Liang Z, et al. Revealing of the ultrafast third-order nonlinear optical response and enabled photonic application in two-dimensional tin sulfide. Photonics Res 2019;7:494–502.
[80] Wu L, Xie Z, Lu L, et al. Few-layer tin Sulfide: a promising black-phosphorus-analogue 2D material with exceptionally large nonlinear optical response, high stability, and applications in all-optical switching and wavelength conversion. Adv Opt Mater 2018;6:1700985.

[81] Zhang Y, Lim C-K, Dai Z, et al. Photonics and optoelectronics using nano-structured hybrid perovskite media and their optical cavities. Phys Rep 2019;795:1–51.
[82] Li P, Chen Y, Yang T, et al. Two-dimensional $CH_3NH_3PbI_3$ perovskite nanosheets for ultrafast pulsed fiber lasers. ACS Appl Mater Inter 2017;9:12759–65.
[83] Zhang Y, Liu J, Wang Z, et al. Synthesis, properties, and optical applications of low-dimensional perovskites. Chem Commun 2016;52:13637–55.
[84] Zhang H, Li Y, Hou J, Du A, Chen Z. Dirac state in the FeB_2 monolayer with graphene-like boron sheet. Nano Lett 2016;16:6124–9.
[85] Ponomarenko L, Schedin F, Katsnelson M, et al. Chaotic Dirac billiard in graphene quantum dots. Science 2008;320:356–8.
[86] Pesin D, MacDonald AH. Spintronics and pseudospintronics in graphene and topological insulators. Nat Mater 2012;11:409.
[87] Bonaccorso F, Sun Z, Hasan T, Ferrari A. Graphene photonics and optoelectronics. Nat Photon 2010;4:611.
[88] Bao Q, Zhang H, Ni Z, et al. Monolayer graphene as a saturable absorber in a mode-locked laser. Nano Res 2011;4:297–307.
[89] Bonaccorso F, Sun Z. Solution processing of graphene, topological insulators and other 2d crystals for ultrafast photonics. Opt Mater Express 2013;4:63–78.
[90] Sobon G. Mode-locking of fiber lasers using novel two-dimensional nanomaterials: graphene and topological insulators. Photonics Res 2015;3:A56–63.
[91] Li W, Chen B, Meng C, et al. Ultrafast all-optical graphene modulator. Nano Lett 2014;14:955–9.
[92] Uddin S, Debnath PC, Park K, Song Y-W. Nonlinear black phosphorus for ultrafast optical switching. Sci Rep 2017;7:43371.
[93] Wang CY, Guo GY. Nonlinear optical properties of transition-metal dichalcogenide MX_2 (M = Mo, W; X = S, Se) monolayers and trilayers from first-principles calculations. J Phys Chem C 2015;119:13268–76.
[94] Eswaraiah V, Aravind SSJ, Ramaprabhu S. Top down method for synthesis of highly conducting graphene by exfoliation of graphite oxide using focused solar radiation. J Mater Chem 2011;21:6800–3.
[95] Wang X, Ning J, Zheng C, et al. Photoluminescence and Raman mapping characterization of WS_2 monolayers prepared using top-down and bottom-up methods. J Mater Chem C 2015;3:2589–92.
[96] Huang X, Zeng Z, Zhang H. Metal dichalcogenide nanosheets: preparation, properties and applications. Chem Soc Rev 2013;42:1934–46.
[97] Yasaei P, Kumar B, Foroozan T, et al. High-quality black phosphorus atomic layers by liquid-phase exfoliation. Adv Mater 2015;27:1887–92.
[98] Kang KN, Godin K, Yang EH. The growth scale and kinetics of WS_2 monolayers under varying H_2 concentration. Sci Rep 2015;5:1–9.
[99] Shaw JC, Zhou H, Chen Y, et al. Chemical vapor deposition growth of monolayer $MoSe_2$ nanosheets. Nano Res 2014;7:511–7.
[100] Vodopyanov KL, Lukashev AV, Phillips CC, Ferguson IT. Passive mode locking and Q switching of an erbium 3 μm laser using thin InAs epilayers grown by molecular beam epitaxy. Appl Phys Lett 1991;59:1658–60.
[101] Yue R, Barton AT, Zhu H, et al. $HfSe_2$ thin films: 2D transition metal dichalcogenides grown by molecular beam epitaxy. ACS Nano 2014;9:474–80.
[102] Shen J, Yan B, Shi M, Ma H, Li N, Ye M. One step hydrothermal synthesis of TiO_2-reduced graphene oxide sheets. J Mater Chem 2011;21:3415–21.
[103] Feng S, Xu R. New materials in hydrothermal synthesis. Accounts Chem Res 2001;34:239–47.
[104] Wang J, Jiang Z, Chen H, et al. High energy soliton pulse generation by a magnetron-sputtering-deposition-grown $MoTe_2$ saturable absorber. Photonics Res 2018;6:535–41.
[105] Voevodin AA, Waite AR, Bultman JE, Hu J, Muratore C. Magnetic field argon ion filtering for pulsed magnetron sputtering growth of two-dimensional MoS_2. Surf Coat Tech 2015;280:260–7.
[106] Yang Z, Hao J, Yuan S, et al. Field-effect transistors based on amorphous black phosphorus ultrathin films by pulsed laser deposition. Adv Mater 2015;27:3748–54.
[107] Bang GS, Nam KW, Kim JY, Shin J, Choi JW, Choi S-Y. Effective liquid-phase exfoliation and sodium ion battery application of MoS_2 nanosheets. Acs Appl Mater Inter 2014;6:7084–9.
[108] Hernandez Y, Nicolosi V, Lotya M, et al. High-yield production of graphene by liquid-phase exfoliation of graphite. Nat Nanotechnol 2008;3:563.
[109] Ciesielski A, Samorì P. Graphene via sonication assisted liquid-phase exfoliation. Chem Soc Rev 2014;43:381–98.
[110] Yu J, Li J, Zhang W, Chang H. Synthesis of high quality two-dimensional materials via chemical vapor deposition. Chem Sci 2015;6:6705–16.
[111] Cai Z, Liu B, Zou X, Cheng H-M. Chemical vapor deposition growth and applications of two-dimensional materials and their heterostructures. Chem Rev 2018;118:6091–133.
[112] Cox JD, Marini A, De Abajo FJG. Plasmon-assisted high-harmonic generation in graphene. Nat Commun 2017;8:14380.
[113] Jakubczyk T, Delmonte V, Koperski M, et al. Radiatively limited dephasing and exciton dynamics in $MoSe_2$ monolayers revealed with four-wave mixing microscopy. Nano Lett 2016;16:5333–9.
[114] Vermeulen N, Castelló Lurbe D, Cheng J, et al. Negative Kerr nonlinearity of graphene as seen via chirped-pulse-pumped self-phase modulation. Phys Rev Appl 2016;6:044006.
[115] Lu S, Zhao C, Zou Y, et al. Third order nonlinear optical property of Bi_2Se_3. Opt Express 2013;21:2072–82.
[116] Wang K, Wang J, Fan J, et al. Ultrafast saturable absorption of two-dimensional MoS_2 nanosheets. ACS Nano 2013;7:9260–7.
[117] Du J, Zhang M, Guo Z, et al. Phosphorene quantum dot saturable absorbers for ultrafast fiber lasers. Sci Rep 2017;7:42357.
[118] Zhang H, Virally S, Bao Q, et al. Z-scan measurement of the nonlinear refractive index of graphene. Opt Lett 2012;37:1856–8.
[119] Sheik-Bahae M, Said AA, Van Stryland EW. High-sensitivity, single-beam n_2 measurements. Opt Lett 1989;14:955–7.
[120] Sheik-Bahae M, Said AA, Wei T-H, Hagan DJ, Van Stryland EW. Sensitive measurement of optical nonlinearities using a single beam. IEEE J Quantum Electron 1990;26:760–9.
[121] Gao Y, Zhang X, Li Y, et al. Saturable absorption and reverse saturable absorption in platinum nanoparticles. Opt Commun 2005;251:429–33.
[122] Hong X, Kim J, Shi SF, et al. Ultrafast charge transfer in atomically thin MoS_2/WS_2 heterostructures. Nat Nanotechnol 2014;9:682–6.
[123] Zhou KG, Zhao M, Chang MJ, et al. Size-dependent nonlinear optical properties of atomically thin transition metal dichalcogenide nanosheets. Small 2015;11:694–701.

[124] Dong N, Li Y, Feng Y, et al. Optical limiting and theoretical modelling of layered transition metal dichalcogenide nanosheets. Sci Rep 2015;5:14646.
[125] Mao D, Cui X, Gan X, et al. Passively Q-switched and mode-locked fiber laser based on an ReS_2 saturable absorber. IEEE J Quantum Electron 2018;24:1100406.
[126] Zhang S, Dong N, McEvoy N, et al. Direct observation of degenerate two-photon absorption and Its saturation in WS_2 and MoS_2 monolayer and few-layer films. ACS Nano 2015;9:7142–50.
[127] Guo B, Lyu Q, Yao Y, Wang P. Direct generation of dip-type sidebands from WS_2 mode-locked fiber laser. Opt Mater Express 2016;6:2475–86.
[128] Zheng X, Zhang Y, Chen R, Xu Z, Jiang T. Z-scan measurement of the nonlinear refractive index of monolayer WS_2. Opt Express 2015;23:15616–23.
[129] Zhang H, Lu SB, Zheng J, et al. Molybdenum disulfide (MoS_2) as a broadband saturable absorber for ultra-fast photonics. Opt Express 2014;22:7249–60.
[130] Zhang R, Zhang Y, Yu H, et al. Broadband black phosphorus optical modulator in the spectral range from visible to mid-infrared. Adv Opt Mater 2015;3:1787–92.
[131] Qin Z, Hai T, Xie G, et al. Black phosphorus Q-switched and mode-locked mid-infrared Er: ZBLAN fiber laser at 3.5 μm wavelength. Opt Express 2018;26:8224–31.
[132] Wang K, Szydłowska BM, Wang G, et al. Ultrafast nonlinear excitation dynamics of black phosphorus nanosheets from visible to mid-infrared. ACS Nano 2016;10:6923–32.
[133] Hanlon D, Backes C, Doherty E, et al. Liquid exfoliation of solvent-stabilized few-layer black phosphorus for applications beyond electronics. Nat Commun 2015;6:8563.
[134] Wang K, Feng Y, Chang C, et al. Broadband ultrafast nonlinear absorption and nonlinear refraction of layered molybdenum dichalcogenide semiconductors. Nanoscale 2014;6:10530–5.
[135] Mao D, Li M, He Z, et al. Optical vortex fiber laser based on modulation of transverse modes in two mode fiber. APL Photonics 2019;4:060801.
[136] Zhang H, Tang D, Zhao L, Bao Q, Loh KP. Vector dissipative solitons in graphene mode locked fiber lasers. Opt Commun 2010;283:3334–8.
[137] Mao D, Zhang S, Wang Y, et al. WS_2 saturable absorber for dissipative soliton mode locking at 1.06 and 1.55 μm. Opt Express 2015;23:27509–19.
[138] Niu K, Sun R, Chen Q, Man B, Zhang H. Passively mode-locked Er-doped fiber laser based on SnS_2 nanosheets as a saturable absorber. Photonics Res 2018;6:72–6.
[139] Li L, Jiang S, Wang Y, et al. WS_2/fluorine mica (FM) saturable absorbers for all-normal-dispersion mode-locked fiber laser. Opt Express 2015;23:28698–706.
[140] Song H, Wang Q, Zhang Y, Li L. Mode-locked ytterbium-doped all-fiber lasers based on few-layer black phosphorus saturable absorbers. Opt Commun 2017;394:157–60.
[141] Hisyam MB, Rusdi MFM, Latiff AA, Harun SW. Generation of mode-locked ytterbium doped fiber ring laser using few-layer black phosphorus as a saturable absorber. IEEE J Quantum Electron 2016;23:39–43.
[142] Xia H, Li H, Lan C, et al. Ultrafast erbium-doped fiber laser mode-locked by a CVD-grown molybdenum disulfide (MoS_2) saturable absorber. Opt Express 2014;22:17341–8.
[143] Zhang M, Howe RCT, Woodward RI, et al. Solution processed MoS_2-PVA composite for sub-bandgap mode-locking of a wideband tunable ultrafast Er:fiber laser. Nano Res 2015;8:1522–34.
[144] Mao D, Wang YD, Ma CJ, et al. WS_2 mode-locked ultrafast fiber laser. Sci Rep 2015;5:7965.
[145] Liu W, Pang L, Han H, et al. Tungsten disulfide saturable absorbers for 67 fs mode-locked erbium-doped fiber lasers. Opt Express 2017;25:2950–9.
[146] Wang Y, Mao D, Gan X, et al. Harmonic mode locking of bound-state solitons fiber laser based on MoS_2 saturable absorber. Opt Express 2015;23:205–10.
[147] Liu M, Zheng XW, Qi YL, et al. Microfiber-based few-layer MoS_2 saturable absorber for 2.5 GHz passively harmonic mode-locked fiber laser. Opt Express 2014;22:22841–6.
[148] Mao D, She X, Du B, et al. Erbium-doped fiber laser passively mode locked with few-layer WSe_2/$MoSe_2$ nanosheets. Sci Rep 2016;6:23583.
[149] Koo J, Park J, Lee J, Jhon YM, Lee JH. Femtosecond harmonic mode-locking of a fiber laser at 3.27 GHz using a bulk-like, MoSe2-based saturable absorber. Opt Express 2016;24:10575–89.
[150] Liu W, Liu M, OuYang Y, Hou H, Lei M, Wei Z. CVD-grown $MoSe_2$ with high modulation depth for ultrafast mode-locked erbium-doped fiber laser. Nanotechnology 2018;29:394002.
[151] Koo J, Jhon YI, Park J, Lee J, Jhon YM, Lee JH. Near-infrared saturable absorption of defective bulk-structured WTe_2 for femtosecond laser mode-locking. Adv Funct Mater 2016;26:7454–61.
[152] Mao D, Du B, Yang D, et al. Nonlinear saturable absorption of liquid-exfoliated molybdenum/tungsten ditelluride nanosheets. Small 2016;12:1489–97.
[153] Chen Y, Jiang G, Chen S, et al. Mechanically exfoliated black phosphorus as a new saturable absorber for both Q-switching and mode-locking laser operation. Opt Express 2015;23:12823–33.
[154] Jin X, Hu G, Zhang M, et al. 102 fs pulse generation from a long-term stable, inkjet-printed black phosphorus-mode-locked fiber laser. Opt Express 2018;26:12506–13.
[155] Li D, Jussila H, Karvonen L, et al. Polarization and thickness dependent absorption properties of black phosphorus: new saturable absorber for ultrafast pulse generation. Sci Rep 2015;5:15899.
[156] Song YF, Li L, Zhang H, Shen de Y, Tang DY, Loh KP. Vector multi-soliton operation and interaction in a graphene mode-locked fiber laser. Opt Express 2013;21:10010–8.
[157] He Z, Zheng Y, Liu H, et al. Passively Q-switched cylindrical vector laser based on a black phosphorus saturable absorber. Chin Opt Lett 2019;17:020004.
[158] Wood JD, Wells SA, Jariwala D, et al. Effective passivation of exfoliated black phosphorus transistors against ambient degradation. Nano Lett 2014;14:6964–70.
[159] Hu G, Albrow-Owen T, Jin X, et al. Black phosphorus ink formulation for inkjet printing of optoelectronics and photonics. Nat Commun 2017;8:1–10.
[160] Feng Q, Liu H, Zhu M, et al. Electrostatic functionalization and passivation of water-exfoliated few-layer black phosphorus by poly dimethyldiallyl ammonium chloride and its ultrafast laser application. ACS Appl Mater Inter 2018;10:9679–87.
[161] Khazaeizhad R, Kassani SH, Jeong H, Yeom DI, Oh K. Mode-locking of Er-doped fiber laser using a multilayer MoS_2 thin film as a saturable absorber in both anomalous and normal dispersion regimes. Opt Express 2014;22:23732–42.

[162] Liu H, Luo AP, Wang FZ, et al. Femtosecond pulse erbium-doped fiber laser by a few-layer MoS_2 saturable absorber. Opt Lett 2014;39:4591–4.
[163] Aiub EJ, Steinberg D, Souza E, Saito LA. 200-fs mode-locked Erbium-doped fiber laser by using mechanically exfoliated MoS_2 saturable absorber onto D-shaped optical fiber. Opt Express 2017;25:10546–52.
[164] Khazaeinezhad R, Kassani SH, Jeong H, et al. Ultrafast pulsed all-fiber laser based on tapered fiber enclosed by few-layer WS_2 nanosheets. IEEE Photonics Tech Lett 2015;27:1581–4.
[165] Liu W, Pang L, Han H, Bi K, Lei M, Wei Z. Tungsten disulphide for ultrashort pulse generation in all-fiber lasers. Nanoscale 2017;9:5806–11.
[166] Zhou B, Liu X, Guo H, et al. Parametrically tunable soliton-induced resonant radiation by three-wave mixing. Phys Rev Lett 2017;118:143901.
[167] Liu X, Pu M, Zhou B, Krückel CJ, Fülöp A, Bache M. Octave-spanning supercontinuum generation in a silicon-rich nitride waveguide. Opt Lett 2016;41:2719–22.
[168] Liu X, Zhou B, Guo H, Bache M. Mid-IR femtosecond frequency conversion by soliton-probe collision in phase-mismatched quadratic nonlinear crystals. Opt Lett 2015;40:3798–801.
[169] Panagiotopoulos P, Whalen P, Kolesik M, Moloney JV. Super high power mid-infrared femtosecond light bullet. Nat Photon 2015;9:543.
[170] Ouzounov D, Freund F. Mid-infrared emission prior to strong earthquakes analyzed by remote sensing data. Adv Space Res 2004;33:268–73.
[171] Antipov S, Hudson DD, Fuerbach A, Jackson SD. High-power mid-infrared femtosecond fiber laser in the water vapor transmission window. Optica 2016;3:1373–6.
[172] Duval S, Bernier M, Fortin V, Genest J, Piché M, Vallée R. Femtosecond fiber lasers reach the mid-infrared. Optica 2015;2:623–6.
[173] de Cumis MS, Viciani S, Borri S, et al. Widely-tunable mid-infrared fiber-coupled quartz-enhanced photoacoustic sensor for environmental monitoring. Opt Express 2014;22:28222–31.
[174] McCarty G, Reeves J, Reeves V, Follett R, Kimble J. Mid-infrared and near-infrared diffuse reflectance spectroscopy for soil carbon measurement. Soil Sci Soc Am J 2002;66:640–6.
[175] Willer U, Saraji M, Khorsandi A, Geiser P, Schade W. Near- and mid-infrared laser monitoring of industrial processes, environment and security applications. Opt Laser Eng 2006;44:699–710.
[176] Nelson L, Ippen E, Haus H. Broadly tunable sub-500 fs pulses from an additive-pulse mode-locked thulium-doped fiber ring laser. App Phys Lett 1995;67:19–21.
[177] Cheng H, Lin W, Luo Z, Yang Z. Passively mode-locked Tm^{3+}-doped fiber laser with gigahertz fundamental repetition rate. IEEE J Quantum Electron 2017;24:1–6.
[178] Shen L, Cai M, Lu Y, et al. Preparation and investigation of Tm^{3+}/Ho^{3+} co-doped germanate-tellurite glass as promising materials for ultrashort pulse laser. Opt Mater 2017;67:125–31.
[179] Antipov S, Jackson SD, Withford MJ, Fürbach A. A passively mode-locked sub-picosecond Ho^{3+}, Pr^{3+}-doped fluoride fiber laser operating at 2.86 μm (Conference Presentation). Fiber Lasers XIV: Technology and Systems: International Society for Optics and Photonics; 2017. p. 100831A.
[180] Tian Z, Wu K, Kong L, et al. Mode-locked thulium fiber laser with MoS_2. Laser Phys Lett 2015;12:065104.
[181] Li J, Luo H, Wang L, et al. 3-μm mid-infrared pulse generation using topological insulator as the saturable absorber. Opt Lett 2015;40:3659–62.
[182] Duan W, Nie H, Sun X, et al. Passively Q-switched mid-infrared laser pulse generation with gold nanospheres as a saturable absorber. Opt Lett 2018;43:1179–82.
[183] You Z, Sun Y, Sun D, et al. High performance of a passively Q-switched mid-infrared laser with Bi_2Te_3/graphene composite SA. Opt Lett 2017;42:871–4.
[184] Cizmeciyan M, Kim J, Bae S, Hong B, Rotermund F, Sennaroglu A. Graphene mode-locked femtosecond Cr: ZnSe laser at 2500 nm. Opt Lett 2013;38:341–3.
[185] Jung M, Lee J, Park J, Koo J, Jhon YM, Lee JH. Mode-locked, 1.94-μm, all-fiberized laser using WS_2-based evanescent field interaction. Opt Express 2015;23:19996–20006.
[186] Qin Z, Xie G, Zhao C, Wen S, Yuan P, Qian L. Mid-infrared mode-locked pulse generation with multilayer black phosphorus as saturable absorber. Opt Lett 2016;41:56–9.
[187] Kara O, Sweeney F, Rutkauskas M, Farrell C, Leburn CG, Reid DT. Open-path mid-infrared remote sensing of atmospheric gases using a broadband optical parametric oscillator. Conference on Lasers and Electro-Optics. San Jose, California: Optical Society of America; 2019. p. AM2K.4.
[188] Li J, Luo H, Zhai B, et al. Black phosphorus: a two-dimension saturable absorption material for mid-infrared Q-switched and mode-locked fiber lasers. Sci Rep 2016;6:30361.
[189] Wang J, Jiang Z, Chen H, et al. Magnetron-sputtering deposited WTe_2 for an ultrafast thulium-doped fiber laser. Opt Lett 2017;42:5010–3.
[190] Lee J, Koo J, Lee J, Jhon YM, Lee JH. All-fiberized, femtosecond laser at 1912 nm using a bulk-like $MoSe_2$ saturable absorber. Opt Mater Express 2017;7:2968–79.
[191] Andrés M, Cruz J, Díez A, Pérez-Millán P, Delgado-Pinar M. Actively Q-switched all-fiber lasers. Laser Phys Lett 2007;5:93.
[192] Zhang H, He J, Wang Z, et al. Dual-wavelength, passively Q-switched Tm:YAP laser with black phosphorus saturable absorber. Opt Mater Express 2016;6:2328–35.
[193] Wu K, Zhang X, Wang J, Li X, Chen J. WS_2 as a saturable absorber for ultrafast photonic applications of mode-locked and Q-switched lasers. Opt Express 2015;23:11453–61.
[194] Yu H, Zheng X, Yin K, Jiang T. Nanosecond passively Q-switched thulium/holmium-doped fiber laser based on black phosphorus nanoplatelets. Opt Mater Express 2016;6:603–9.
[195] Al-Masoodi A, Ahmed M, Latiff A, Arof H, Harun SW. Q-switched ytterbium-doped fiber laser using black phosphorus as saturable absorber. Chin Phys Lett 2016;33:054206.
[196] Chu Z, Liu J, Guo Z, Zhang H. 2 μm passively Q-switched laser based on black phosphorus. Opt Mater Express 2016;6:2374–9.
[197] Chen B, Zhang X, Wu K, Wang H, Wang J, Chen J. Q-switched fiber laser based on transition metal dichalcogenides MoS_2, $MoSe_2$, WS_2, and WSe_2. Opt Express 2015;23:26723–37.
[198] Li W, Peng J, Zhong Y, et al. Orange-light passively Q-switched Pr^{3+}-doped all-fiber lasers with transition-metal dichalcogenide saturable absorbers. Opt Mater Express 2016;6:2031–9.
[199] Woodward RI, Kelleher EJ, Howe RC, et al. Tunable Q-switched fiber laser based on saturable edge-state absorption in few-layer molybdenum disulfide (MoS_2). Opt Express 2014;22:31113–22.

[200] Luo Z, Huang Y, Zhong M, et al. 1-, 1.5-, and 2-μm Fiber Lasers Q-Switched by a Broadband Few-Layer MoS2 Saturable Absorber. J Lightwave Technol 2014;32:4077–84.
[201] Yu H, Zheng X, Yin K, Cheng Xa, Jiang T. Nanosecond passively Q-switched thulium/holmium-doped fiber laser based on black phosphorus nanoplatelets. Opt Mater Express 2016;6:603–9.
[202] Wei R, Zhang H, Hu Z, et al. Ultra-broadband nonlinear saturable absorption of high-yield MoS_2 nanosheets. Nanotechnology 2016;27:305203.
[203] Chen JH, Deng GQ, Yan SC, et al. Microfiber-coupler-assisted control of wavelength tuning for Q-switched fiber laser with few-layer molybdenum disulfide nanoplates. Opt Lett 2015;40:3576–9.
[204] Xia H, Li H, Lan C, et al. Few-layer MoS_2 grown by chemical vapor deposition as a passive Q-switcher for tunable erbium-doped fiber lasers. Photonics Res 2015;3: A92–A6.
[205] Huang Y, Luo Z, Li Y, et al. Widely-tunable, passively Q-switched erbium-doped fiber laser with few-layer MoS_2 saturable absorber. Opt Express 2014;22:25258–66.
[206] Ren J, Wang S, Cheng Z, et al. Passively Q-switched nanosecond erbium-doped fiber laser with MoS_2 saturable absorber. Opt Express 2015;23:5607–13.
[207] Lin J, Hu Y, Chen C, Gu C, Xu L. Wavelength-tunable Yb-doped passively Q-switching fiber laser based on WS_2 saturable absorber. Opt Express 2015;23:29059–64.
[208] Lin J, Yan K, Zhou Y, Xu LX, Gu C, Zhan QW. Tungsten disulphide based all fiber Q-switching cylindrical-vector beam generation. Appl Phys Lett 2015;107:191108.
[209] Woodward RI, Howe RC, Runcorn TH, et al. Wideband saturable absorption in few-layer molybdenum diselenide ($MoSe_2$) for Q-switching Yb-, Er- and Tm-doped fiber lasers. Opt Express 2015;23:20051–61.
[210] Liu W, Liu M, Lei M, Fang S, Wei Z. Titanium selenide saturable absorber mirror for passive Q-switched Er-doped fiber laser. IEEE J Quantum Electron 2017;24:1–5.
[211] Wu D, Cai Z, Zhong Y, et al. Compact passive Q-switching Pr^{3+}-doped ZBLAN fiber laser with black phosphorus-based saturable absorber. IEEE J Quantum Electron 2016;23:7–12.
[212] Huang K, Lu BL, Li D, et al. Black phosphorus flakes covered microfiber for Q-switched ytterbium-doped fiber laser. Appl Opt 2017;56:6427–31.
[213] Mu H, Lin S, Wang Z, et al. Black phosphorus–polymer composites for pulsed lasers. Adv Opt Mater 2015;3:1447–53.
[214] Qin Z, Xie G, Zhang H, et al. Black phosphorus as saturable absorber for the Q-switched Er: ZBLAN fiber laser at 2.8 μm. Opt Express 2015;23:24713–8.
[215] Ma C, Wang C, Gao B, Adams J, Wu G, Zhang H. Recent progress in ultrafast lasers based on 2D materials as a saturable absorber. App Phys Rev 2019;6:041304.
[216] Tan W, Su C, Knize R, Xie G, Li L, Tang D. Mode locking of ceramic Nd: yttrium aluminum garnet with graphene as a saturable absorber. Appl Phys Lett 2010;96:031106.
[217] Zhang B, Lou F, Zhao R, et al. Exfoliated layers of black phosphorus as saturable absorber for ultrafast solid-state laser. Opt Lett 2015;40:36ww91–4.
[218] Mary R, Brown G, Beecher SJ, et al. 1.5 GHz picosecond pulse generation from a monolithic waveguide laser with a graphene-film saturable output coupler. Opt Express 2013;21:7943–50.
[219] Choudhary A, Beecher SJ, Dhingra S, et al. 456-mW graphene Q-switched Yb: yttria waveguide laser by evanescent-field interaction. Opt Lett 2015;40:1912–5.